JACS
JOURNAL OF THE AMERICAN CHEMICAL SOCIETY
Article
pubs.acs.org/JACS

Reconstructive Transitions from Rotations of Rigid Heteroanionic Polyhedra

Michael Holland,[†] Nenian Charles,[‡] James M. Rondinelli,[§] and Kenneth R. Poeppelmeier*[,†,§]

[†]Department of Chemistry, Northwestern University, Evanston, Illinois 60208, United States
[‡]Department of Materials Science and Engineering, Drexel University, Philadelphia, Pennsylvania 19104, United States
[§]Department of Materials Science and Engineering, Northwestern University, Evanston, Illinois 60208, United States

Supporting Information

ABSTRACT: Phase transitions are ubiquitous in structurally complex transition metal compounds composed of homoanionic polyhedra, including nitrides, oxides, and fluorides. The symmetry breaking that occurs across polymorphic transitions is often achieved by small atomic displacements, rendering these displacive transitions reversible. In contrast, elemental crystals, alloys, and simple minerals will exhibit reconstructive "bond-breaking" transitions. Here we show that a reconstructive transition occurs in the heteroanionic compound $KNaNbOF_5$, owing to reorientations of the $[NbOF_5]^{2-}$ units that trigger a reconfiguration of the cation lattice. Using a combination of synchrotron-based measurements, empirical dynamic simulations, and *ab initio* calculations, we report structure changes across the transition and formulate an atomistic minimum energy transition path to explain its irreversible nature. Our results indicate that multianionic compounds are likely to host reconstructive transitions that are frequently difficult to study and functionalize in simpler compounds. We anticipate that our insight into the forces that drive the transition will also lead to novel methods to control the assembly of structures in the solid state.

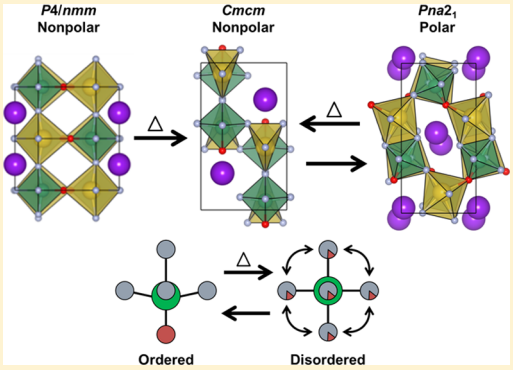

INTRODUCTION

Investigating crystalline solid−solid phase transitions enhances our understanding of inorganic structures and guides synthetic stabilization of new polymorphs. Critical transition temperatures and pressures provide insights into relative stabilities and transition pathways among competing phases in the potential energy landscape and the effective interatomic interactions underlying transition domains. In complex inorganic systems, reconstructive transitions are of particular interest because they are both rare and challenging to characterize.[1] The main features of reconstructive transitions are the absence of a group−subgroup symmetry relationship between phases and large atomic displacements that involve high activation barriers.[2,3] Owing to the energy involved in chemical bond breaking, reconstructive transitions usually occur under conditions that make time-resolved experimental methods impractical; therefore, when studying such transitions, theoretical techniques or phenomenological models are applied.[4−7]

Reconstructive transitions "of any kind" are generally regarded as rare exceptions, with most transitions being displacive, i.e., involving small atomic displacements, in chemically complex compounds (ternary or higher) composed of homoanionic transition metal (M) polyhedra such as oxides (MO_6, MO_5, MO_4), sulfides (MS_6, MS_5), and fluorides (MF_6).[1] The dearth of reconstructive transitions in these compounds is attributed to the strong competition between atomic displacements in adjacent cationic and anionic sublattices that act to preserve a group−subgroup relationship.[1] Although a few notable examples of reconstructive transitions occur in ternary compounds under geological or experimentally imposed conditions, including the perovskite-to-post-perovskite transition in $CaBO_3$ (B = Ru, Rh, Sn, Ir), monoclinic-to-orthorhombic transitions in K_2ZnBr_4 and K_2CoBr_4, the zircon-to-scheelite transition in $ZrSiO_4$,[8−10] and likely the spinel-to-post-spinel transition[11] in Fe_3O_4, by far most reported polymorphic transitions in homoanionc compounds at technologically relevant pressures and temperatures are displacive.

In the case of heteroanionic compounds with two or more anionic species, the frequency and tendency for reconstructive rather than displacive transitions to occur is poorly understood despite recent interest in tuning the electronic, magnetic, and optical properties of oxynitride, oxypnictide, and oxyhalide compounds.[12−14] Here we identify a laboratory-accessible, temperature-induced, reconstructive transition in the multianionic compound $KNaNbOF_5$ by employing a combination of *in situ* and synchrotron powder X-ray diffraction (XRD) measurements, *ab initio* computational methods, and molecular dynamics (MD) simulations using a uniquely derived set of interatomic potentials based on cryogenic diamond anvil cell (DAC) synchrotron single-crystal XRD. We show that the

Received: July 1, 2016
Published: August 17, 2016

DOI: 10.1021/jacs.6b06813
J. Am. Chem. Soc. 2016, 138, 11882−11889

reconstructive transition occurs between two centrosymmetric structures with an anion-ordered *P*4/*nmm* (low-temperature, LT) and anion-disordered *Cmcm* (high-temperature, HT) symmetry; the latter is determined for the first time through computationally proposed structures, based on the results of our MD simulations, utilized in systematic powder XRD comparisons. The transition is driven by a reorientation of the $[NbOF_5]^{2-}$ units, which disorder upon heating. Increasing temperature effectively decouples the $[NbOF_5]^{2-}$ units from the alkali metal sublattices, which allows the "rigid" molecular-like $[NbOF_5]^{2-}$ units to undergo hopping rotations, altering the O and F site order, and spurs reconfiguration of occupied alkali cation sites. We use *ab initio* calculations to devise a model pathway for the reconstructive transition and approximate its energetic barrier, which strongly supports the notion that the transition originates from the chemistry of the heteroanionic $[NbOF_5]^{2-}$ units. Understanding the transition between polymorphs, in particular the interplay between cation sublattices and heteroanionic units that preferentially stabilize specific crystal polymorphs, will bring us closer to directed synthesis of new inorganic materials with desired structural features.

RESULTS AND DISCUSSION

Polymorphs Participating in the Transition. The $KNaNbOF_5$ exhibits two polymorphs at room temperature:[15] a centrosymmetric (CS) structure crystallizing in space group *P*4/*nmm* and a polar non-centrosymmetric (NCS) structure in space group $Pna2_1$ (Figure 1). Interesting nonlinear properties

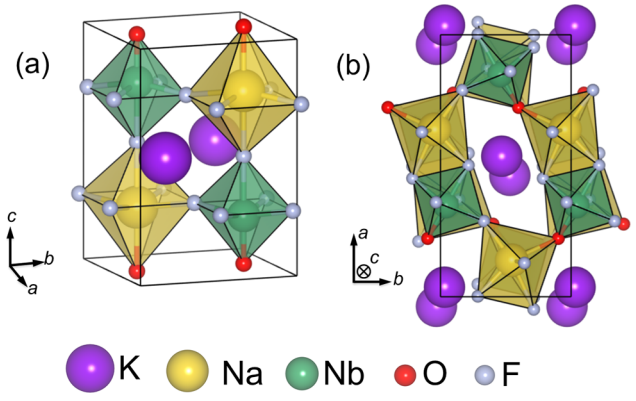

Figure 1. Unit cells for known phases of $KNaNbOF_5$: (a) *P*4/*nmm* (CS) structure and (b) $Pna2_1$ (NCS) structure.

of the NCS phase have been investigated both experimentally and by *ab initio* theoretical methods.[16,17] Importantly, the polymorphs of $KNaNbOF_5$ are quite distinct from each other. The CS phase has a perovskite-like structure and a higher degree of order in the orientation the $[NbOF_5]^{2-}$ anionic units. Additionally, there is no K−O coordination in the CS phase, but there is K−O coordination in the NCS phase.

Our *in situ* XRD experiments discovered a previously unreported HT phase bridging the two room-temperature structures at ∼360 °C.[17,18] We observe that, upon heating, the CS and NCS phases both transform to the same HT phase. However, $KNaNbOF_5$ always reverts to the NCS phase upon cooling. The transition from the CS to NCS structure is likely to involve two separate sequences. First, an *irreversible* transition connects the *P*4/*nmm* CS structure to the "bridging", and previously unsolved, HT transition phase. Second, a reversible transition links the HT phase to the NCS phase. Attempts were made to index and solve the HT structure from the *in situ* powder XRD data, but the results were inconclusive.[17,18] The stark contrast between the structures of the two stable polymorphs, and the first-order behavior of the transitions (Supplementary Figure 1), indicate that $KNaNbOF_5$ likely undergoes a reconstructive phase transition from the CS to the HT phase. The lack of structural information on the HT phase adds to the complexity involved in understanding the transition processes.

To address the reconstructive nature of the CS-to-HT transition in $KNaNbOF_5$, identification of the HT structure bridging the CS and NCS phases is required. To this end, we first performed MD simulations to rapidly explore the accessible phase space with a uniquely parametrized set of empirical pairwise interatomic interaction functions (see Methods). Our parametrization method used cryogenic (T = 15 K) DAC single-crystal diffraction studies of the lattice and atomic position parameters of $KNaNbOF_5$ over a range of pressures (Figure 2). The crystal structures solved with

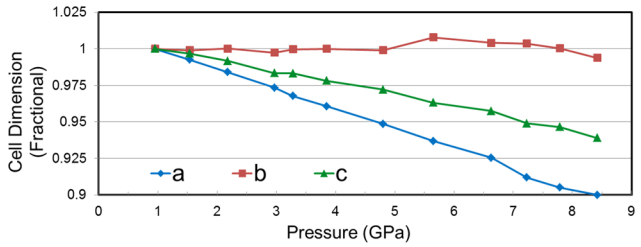

Figure 2. Experimentally observed changes in the lattice dimensions of the NCS phase with pressure at 15 K by cryogenic DAC single-crystal diffraction at Argonne National Laboratory. The crystal volume decreases approximately linearly with increasing pressure. In several regions the *b*-axis length expands with increasing pressure. The *b*-axis is longer than its initial value through the 5−8 GPa range, and over the explored pressure range it changes only very slightly in comparison to the *a*-axis and *c*-axis. *Error in the y-axis is too small to depict.*

reasonable confidence (R < 0.15) are available in the Supporting Information. We then fit interatomic interaction function parameters to these LT pressure-dependent crystal structures. By fitting potential parameters to structures collected at such low temperatures, the impact of thermal vibrations on the measured (and fit) interatomic distances was minimized. We then used the resulting empirical pair potentials to perform finite-temperature MD simulations of $KNaNbOF_5$ at atmospheric pressure.

Figure 3 plots the root-mean-square differences between the simulated lattice dimensions, in the form of a 1 ps moving average, compared to the unit cell dimensions for three experimental polymorphs against simulation time. (Note that for the HT structure, we use an orthorhombic cell fit to the most intense peaks of the experimental powder pattern.) During the simulation, two distinct structures appear with lattice dimensions matching the experimental powder diffraction pattern of the HT phase, and these were further investigated as plausible crystal structures of the HT phase.

The candidate *Pbcm* and *Pnma* space groups for the HT phase, which include complete crystallographic data, i.e., occupied Wyckoff orbits of the different ions, were obtained using snapshots from the MD simulation (with *P*1 symmetry) and the symmetry-identifying tool, FindSym.[19] The provided

DOI: 10.1021/jacs.6b06813
J. Am. Chem. Soc. 2016, 138, 11882−11889

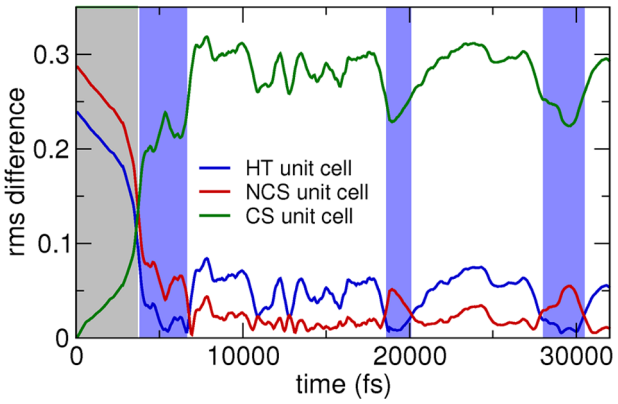

Figure 3. Plot of root-mean-square differences between the simulated crystal lattice parameters as a 1 ps moving average and the lattice parameters for the three experimentally observed phases against simulation time; the phase with the lowest value is the phase with the unit cell parameters that most closely match those of the simulated cell at that time. The simulation is observed to transition from the CS phase to a HT phase and then to transition multiple times between HT phases and the NCS phase. The gray highlighted region indicates the period when the simulation was constrained to promote the initial transition, and the blue highlighted regions indicate periods when candidate structures for the HT phase were observed. The simulation temperature was held constant at 350 °C.

structures exhibit artificially ordered $[NbOF_5]^{2-}$ anions without the local O/F site disorder that we observed in the simulation snapshots. The O/F disorder was removed to facilitate investigation of the structures by DFT methods. Careful comparison between the experimental powder XRD and simulated *Pbcm* and *Pnma* patterns of the HT phase revealed several low-intensity peaks in each simulated pattern not represented in the experimental pattern (Figure 4). These unrepresented peaks indicate that the experimental HT phase has higher symmetry than either of the structures we identified from the simulation. Consequently, we investigated the possibility that the experimental HT phase could be a dynamically disordered system. In other words, the HT phase at the unit cell level consists of a disordered mixture of the *Pbcm* and *Pnma* phases with disordered $[NbOF_5]^{2-}$ anions. Although during our MD simulation the O and F sites disorder, we eliminate this specific site configurational degree of freedom to obtain an idealized HT crystal structure that maintains a supergroup relationship to the artificially ordered *Pbcm* (space group no. 57) and *Pnma* (no. 60) phases. The minimal supergroups of *Pbcm* and *Pnma* that are consistent with the lattice orthorhombicity were found to be *Cmcm* (no. 63), *Cmce* (no. 64), and *Pbcm* (no. 57); we omit the latter since this alternate *Pbcm* structure requires a cell multiplication that is not observed experimentally. Symmetry analysis of the cation-only sublattices, i.e., removal of the anionic groups, for both the *Pbcm* and *Pnma* structures yields a structure with *Cmcm* symmetry. On this basis, we then eliminated the *Cmce* phase as a potential HT structure.

Next, the complete *Cmcm* $KNaNbOF_5$ structure is obtained by populating anion sites approximately midway between those of the *Pnma* and *Pbcm* unit cells with O and F to maintain the $[NbOF_5]^{2-}$ and performing total energy density functional calculations to optimize the positions of all sites at the experimentally observed HT lattice parameters. The related ordered *Cmcm* structure consists of the rigid $NbOF_5$ octahedral units that are somewhat dilated (polyhedral volume of ~9.75 $Å^3$) compared to the LT *P4/nmm* structure. It also exhibits unfavorable 5-fold coordinated Na cations, which are discussed in detail below, and chains of K^+ ions along *c* filling the cavities created in the *ab* planes formed by the corner-connected $[NaF_5]^{4-}$ and $[NbOF_5]^{2-}$ anionic groups (Supplementary Figure 2).

The simulated powder diffraction pattern of this optimized *Cmcm* structure was compared to the experimental HT phase pattern (Figure 4). We find excellent agreement among the peak intensities, and only two of the low-intensity *Cmcm* simulated diffraction peaks were absent from the experimental pattern. (Note that besides these two peaks, several reflections found in the experimental pattern but missing in the simulated pattern were matched with various silicates that could arise as minor components from side reactions between the sample and glass wool used in the experimental setup.) We found that the extra peaks from the idealized *Cmcm* with ordered $[NbOF_5]^{2-}$ anionic groups could be eliminated from the simulated pattern by treating the O and F sites as disordered, which also involves removing the corresponding Nb out-of-center displacements (Supplementary Figure 3). This analysis and agreement between the model HT phase and the experimental powder XRD support the notion that the experimental HT phase

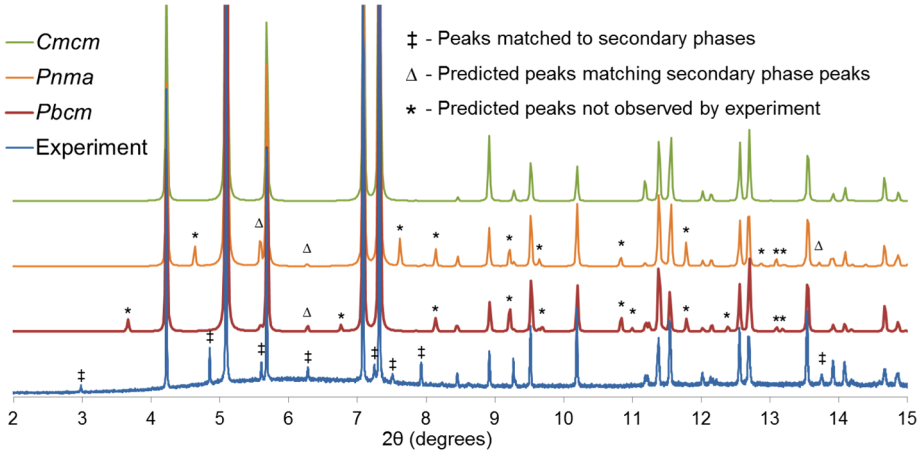

Figure 4. Comparison of experimental powder XRD pattern for the HT phase of $KNaNbOF_5$, simulated patterns for the two candidate phases (*Pbcm* and *Pnma*) identified from our MD simulation, and simulated pattern for the proposed average structure for the HT phase (*Cmcm*).

DOI: 10.1021/jacs.6b06813
J. Am. Chem. Soc. 2016, 138, 11882−11889

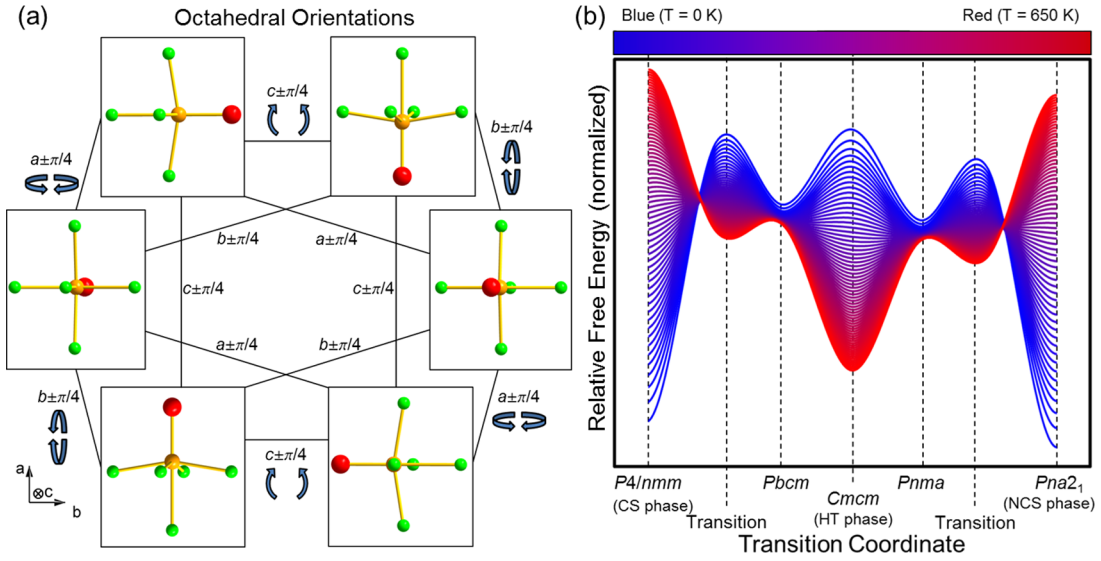

Figure 5. (a) Polar $[NbOF_5]^{2-}$ octahedra undergo 90° hopping rotations at a rate determined by the temperature of the system. The rotational axes relating pairs of the six stable orientations are indicated. These hopping rotations lead to disorder of the O and F sites, and they effectively lower the strength of O^{2-} and F^- bonds with K^+ and Na^+ ions. The order−disorder transition is continuous. (b) A qualitative transition-state theory plot illustrating the influence of temperature-driven octahedral disorder on the free energy landscape of the $KNaNbOF_5$ system. Line colors from blue to red indicate the temperature (in 10 K increments). When the $[NbOF_5]^{2-}$ octahedra are ordered (at low temperature, blue lines), the CS and NCS phases are stable, but as the temperature rises and the degree of octahedral disorder increases, the *Cmcm* phase that is observed at HT conditions becomes favored. The zero-temperature free energy landscape (last blue line) is identical to the potential energy landscape combined with contributions from the zero-point energy. The *Cmcm* phase is a transition state and an unstable phase in the potential energy landscape, while in the free energy landscape it becomes the stable phase at high temperature.

exhibits *Cmcm* symmetry with dynamically disordered $[NbOF_5]^{2-}$ anions.

Disorder from Rigid Heteroanionic Units. Polar, anionic $[NbOF_5]^{2-}$ units are held together by the strongest bonds in the $KNaNbOF_5$ system, and these anionic units are expected to remain intact through both phase transitions. From reported properties of related compounds, it is expected that thermal dissociation of the $[NbOF_5]^{2-}$ anion happens at temperatures in excess of 600 °C, more than 200 °C higher than the highest experimental temperature used for this work.[20] We observed frequent occurrences of 90° "hopping"-type rotations of $[NbOF_5]^{2-}$ octahedral units in the course of our MD simulations (Supplementary Figure 4). Figure 5a shows the different stable orientations and the rotations relating them. Previous work on the compound $K_3WO_3F_3$ produced compelling experimental evidence for temperature-driven reorientations of polar, heteroanionic octahedra leading to displacive order−disorder transitions.[21] In our compound, these rotation events reorient the dipole moment of the $[NbOF_5]^{2-}$ unit with respect to the extended cation lattice, causing the observed O and F site disorder discussed above, and play a key role in phase transition processes: When the $[NbOF_5]^{2-}$ octahedra throughout the extended structure are distributed between the six orientations depicted in Figure 5a, but the temperature is low enough that the time between rotation events for individual octahedra is longer than the time scale of measurement, the system is statically disordered. When the temperature is high enough that the mean time between reorientation events is short compared to the time scale of the measurement, the system is dynamically disordered. As the temperature of the system increases, the degree of dynamic disorder also increases, because rotational hopping of $[NbOF_5]^{2-}$ units result from thermal vibrations, and these rotations produce O and F site disorder.

Although phase transitions in related oxyfluoride elpasolites can also be driven by reorientations or "rotations" of heteroanionic units, they are generally displacive order−disorder type as opposed to reconstructive.[21−24] To understand why the transition here is reconstructive, we must recognize that these rotations produce an O/F site order−disorder transition that intimately couples with the arrangement of the alkali metal sublattice. Similar to a double perovskite, the CS *P4/nmm* structure has two 12-coordinate sites, one occupied by K^+ cations while the other is vacant. In the CS phase, O and F ordering stabilizes the observed ordering of K^+ cations and vacant sites. When the O and F sites in this phase become disordered (upon heating), the K^+ and vacant site order is destabilized by the changes in the anion coordination. A consequent rearrangement of the cation sublattice is driven by electrostatic repulsion between occupied K^+ sites, which combine with the vacant sites, resulting in the observed reconstructive transition. In this way, the dynamic disorder from the $[NbOF_5]^{2-}$ units, within the framework of the cation sublattice, acts as a gateway for the reconstructive transition. In contrast, reconstructive transitions do not occur in the oxyfluoride elpasolites, despite their strong similarity to the CS structure, because the elpasolite composition lacks the vacant cation sites necessary for the destabilization mechanism.

Irreversible Transition. To explain the irreversibility of the transition, we *qualitatively* describe the evolution of the polymorphs using a transition-state theory model (Figure 5b). The free energy values are shifted and rescaled to show the changes in relative free energy among various structures. The difference between the free energy landscape, which includes finite temperature contributions, and the potential energy landscape is an important one. The potential energy landscape includes only electronic contributions, while the free energy landscape combines electronic contributions with vibrational

DOI: 10.1021/jacs.6b06813
J. Am. Chem. Soc. 2016, 138, 11882−11889

and configurational entropic effects. Consequently, as the temperature of a system decreases, the free energy landscape approaches the potential energy landscape. Systems achieve equilibrium by minimizing their free energy. A quantitative plot of theoretical predictions for the temperature-dependent free energies of the *P*4/*nmm*, transition state C from the calculated minimum energy pathway (discussed below), *Pbcm*, and *Cmcm* structures is available in Supplementary Figure 7.

We augment this analysis with a description of the effects of temperature-dependent disorder of the $[NbOF_5]^{2-}$ dipole orientations. This disorder changes the potential energy of structures as well as the free energy. In the low-temperature ordered state, the CS phase exists as a metastable structure in the potential energy landscape as the polar NCS structure is more stable (Figure 5b). When the $[NbOF_5]^{2-}$ octahedra are disordered, the coordination environment of the layered K^+ cations and vacant cation sites in the CS phase lose the stabilizing influence of that order. The result is that the K^+ sites and vacant sites develop opposite effective charges and begin to mutually attract. The HT phases (*Pbcm*, *Pnma*, and *Cmcm*) are stabilized because the K^+ and vacancies are combined in these structures. At high temperature, with fully disordered $[NbOF_5]^{2-}$ octahedra and sufficient thermal energy, the free energy of the CS-to-HT transition is reduced, and the *Pbcm* and *Pnma* phases, which are locally stable variants of *Cmcm* in the *potential* energy landscape, become unstable phases in the *free* energy landscape. Thermodynamic equilibrium requires minimization of the *free* energy. Consequently, the *Cmcm* phase is made the stable bulk phase as a dynamically disordered state. Thermally driven octahedral rotations cause the HT structure to be dynamically disordered between the *Pbcm* and the *Pnma* phases. Consequently, even though the experimentally observed HT *Cmcm* structure occupies a saddle point in the potential energy landscape, because it serves as the bridge between the two locally stable polymorphs it is stabilized at high temperature. The HT phase does not revert to the CS phase upon cooling because the CS phase is higher in energy while the system is disordered, and the energy to rearrange the cation sublattice is too high to overcome when the system is cooled enough to become ordered. The HT-to-NCS transition changes the cation sublattice only slightly and remains thermally accessible as the system cools. So the CS-to-HT phase transition is made favorable by octahedral disorder at elevated temperatures (~625 K). Without disorder (only present at elevated temperatures), the CS-to-HT transition is inaccessible, but without ordered octahedra (only possible at low temperatures), the HT phase is more stable than the CS phase. Consequently, the CS-to-HT phase transition is irreversible, and the HT phase always transforms to the NCS phase on cooling.

Transition Pathway. Next, we examine the energetics of the transition using the model *Cmcm* structure, which omits the O and F site disorder but, as we show, captures the bond breaking caused by rotation of the $NbOF_5$ octahedra. We compute a hypothetical minimum energy pathway (MEP) at 0 K between the *P*4/*nmm* and *Cmcm* phases using the generalized solid-state nudged elastic band (G-SSNEB) within a constrained subspace spanned by the *Pbcm* group, which is a common subgroup of both the low-temperature CS and HT phases. The optimized MEP and structures corresponding to points along the reaction coordinate traversing the *Pbcm* subspace are given in Figure 6. Two energetic barriers at ~400 meV/f.u. higher in energy than the low-temperature CS

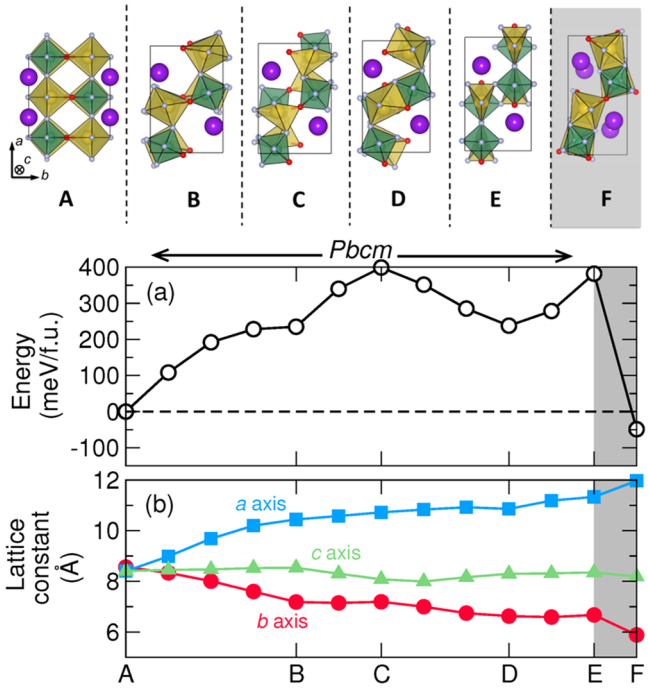

Figure 6. Properties and structure along the minimum energy phase transformation path at zero pressure. The reaction coordinate is accumulated configurational change along the path. Here the letters indicate key structures, shown above. The region shaded gray represents the reversible HT-to-NCS transition not investigated by the G-SSNEB.

structure (reaction coordinate A) appear at reaction coordinates C and E (E corresponds to the HT *Cmcm* structure). An intermediate energetic minimum (~200 meV/f.u.) appears at the coordinate labeled D, and that structure is strikingly similar to the *Pbcm* HT structure obtained from our MD simulations. An energetic inflection point is evident at coordinate B. We attribute this inflection point to the boundary between transition structures with 6-fold and 5-fold Na^+ coordination. At coordinate D, the Na^+ ions regain their 6-fold coordination with a corresponding decrease in energy. The energy of the structure increases again along the transition to point E, where Na^+ is once again 5-fold coordinated.

The evolution of the energy along the MEP can be understood by close examination of the corresponding structures. First, throughout the transformation, the Nb atoms maintain 6-fold coordination ,and the $[NbOF_5]^{2-}$ units act like single-molecule anions owing to the strong hybridization between the Nb 4d states and ligand 2p states (Supplementary Figure 8). The $[NbOF_5]^{2-}$ units undergo rigid 90° counterclockwise rotations about the *c* axis with respect to the units in the neighboring plane. As the $NbOF_5$ octahedra begin to rotate, the Na–ligand bonds are stretched, for example, as would be the case upon heating (A → B), deforming the stable octahedral coordination environment around the Na cation and resulting in an elastic energy penalty. The cell parameters respond to the atomic reconstruction by removing the tetragonality of the *P*4/*nmm* structure. Upon further rotation (B → C), the Na cation coordination is reduced to 5-fold at the maximum (C) owing to a broken Na–F bond. Because stable compounds with 5-coordinate Na are extremely rare, it is understandable that such a structure would correspond to a maximum in the energy landscape. The

DOI: 10.1021/jacs.6b06813
J. Am. Chem. Soc. 2016, 138, 11882–11889

preferred 6-coordinate Na coordination is momentarily recovered after further rotation of the $[NbOF_5]^{2-}$ units through a change in the polyhedral connectivity, i.e., corner-to-edge sharing (A versus D), which lowers the energy of the structure, corresponding to the intermediate minimum at D. The *Cmcm* structure at E is then reached after an additional Na bond breaking, which gives a $KNaNbOF_5$ structure with corner-connectivity but unstable 5-coordinate Na. From A to E, the *b*-axis contracts by ∼2.68 Å, while the *a*-axis elongates by ∼3.56 Å. In contrast, the evolution of the *c*-axis is less drastic, only decreasing by ∼0.22 Å (Figure 6b), which is consistent with the experimental structure evolution and the behavior of the MD simulation.

The most dramatic change that takes place during the transition involves a fundamental restructuring of the cation lattice. We observe in the MEP that K^+ cations are displaced along the *a*-axis, away from the cell boundary, toward the *a*/4 position. In the *P*4/*nmm* structure, the cation lattice includes vacant sites very similar to the K^+ cation sites. By shifting to the *a*/4 position, the K^+ cations are effectively combining with the vacant sites, and thereby eliminating the vacant sites, and changing the cation sublattice to a more densely packed system.

Our results suggest that strong covalent interactions are dominant over ionic bonds in determining the behavior of $KNaNbOF_5$. The strongly covalent nature of the Nb−ligand bonds throughout the MEP reinforces the model that the $[NbOF_5]^{2-}$ octahedra are effectively rigid units throughout the reconstructive transition (Supplementary Figure 9). Conversely, the nearly pure ionic character of the K/Na−ligand bonds reinforces the microscopic view that these bonds are the ones that break over the course of the reconstructive transition. We emphasize that the MEP model is an approximate description of the reconstructive transition in $KNaNbOF_5$. Owing to the first-order nature of the transition, which requires nucleation and growth of the HT phase at the expense of the low-temperature CS phase, the transition is likely to proceed via a domino-like effect that invokes the MEP, as previously discussed, among neighboring unit cells in the structure. The MEP model predicts that the *Pbcm*-type structure, independently observed in the MD simulation, is a local energetic minimum. The *Cmcm* structure is the supergroup transition path linking the *Pbcm* and the *Pnma* structures. Thermal vibration in the crystal lowers the transition energy of this *Cmcm* pathway and generates dynamic disorder along it. The observed HT phase is therefore a realistic *Cmcm* structure that possesses dynamic disorder.

METHODS

Cryogenic Crystallography. Single-crystal XRD precession data were collected for the NCS phase of $KNaNbOF_5$. Single crystals of the NCS phase of $KNaNbOF_5$ were synthesized using a previously reported method.[18] Cryogenic, high-pressure single-crystal diffraction experiments were done using a DAC with rhenium metal gaskets and were performed at station 16-BM-D at the Advanced Photon Source (APS) at Argonne National Laboratory. A liquid helium flow was used to achieve a temperature of 15 K for all experiments. The pressure in the DAC was controlled using a dual diaphragm arrangement and monitored by in-line ruby fluorescence. Experimental pressures ranged from 1 to 10 GPa. Diffraction patterns were collected on a MAR 345 CCD plate detector. Neon gas was used as the pressure medium, and diffraction rings from its crystalline phase can be observed in the collected data. Single-crystal DAC data processing was performed using the GSE_ADA software package and refined using SHELXL.[25,26]

Molecular Dynamics. MD simulations for this project were performed using a purpose-made script written in Mathematica 9. The MD system comprised a pseudo-isothermal−isobaric (NPT) ensemble in which the calculated temperature and internal pressure were fractionally adjusted toward set values with each time step. Internal temperature was calculated from the kinetic energy of the simulated atoms, and pressure was calculated as a sum of contributions from each pair interaction. The supercell angles were fixed at 90°, but each dimension was allowed to change dynamically to adjust the internal pressures by a method analogous to that described by Parrinello and Rahman.[27] Our simulation also introduced very small, randomized fluctuations in atomic momentum vectors intended to mimic radiative thermal energy exchange between ions and accelerate phase space exploration.

$KNaNbOF_5$ is an ionic system. Pairwise interatomic interaction functions can reasonably be applied to dynamic simulations of ionic systems because electrons are primarily localized around individual atoms.[20] We fit an empirical set of pair interaction functions for the $KNaNbOF_5$ system to apply to our MD simulation. We used a multiple power law form for our pair interaction functions, and the force form is given as eq 1. In this equation, r_{ij} is the interatomic

$$F(r_{ij}) = k_e\frac{q_i q_j}{r_{ij}^{\,2}} + \frac{A_{ij}}{r_{ij}^{\,4}} + \frac{B_{ij}}{r_{ij}^{\,6}} + \frac{C_{ij}}{r_{ij}^{\,8}} + \frac{D_{ij}}{r_{ij}^{\,10}} \quad (1)$$

distance between the *i*th and the *j*th ions, k_e is Coulomb's constant (14.39964 V^2 Å eV^{-1}), and the *q* terms are the nominal ionic charges for the two ions. The *A*, *B*, *C*, and *D* terms are the empirical pair function parameters specific to the ion types for *i* and *j*. The first part of this equation is the Coulomb contribution to the pair interaction, and the four other terms are the fitted portion. The fitted sections are purely empirical and are not intended to individually represent specific physical contributions to the interaction. Table S2 gives the numerical values of the empirical constants, *A*, *B*, *C*, and *D*, for each of the 15 pair interaction types.

To increase the predictive range of our pair functions, we fit their empirical parameters to experimental single-crystal structures collected over a range of pressures and exclusively at cryogenic temperatures. We incorporated structure data obtained using DAC variable-pressure, cryogenic diffraction measurements on a sample of the NCS phase of $KNaNbOF_5$. The pair interaction functions were optimized to reproduce, as closely as possible, the atom positions and internal pressures for each experimental structure. Low-temperature (≤100 K) data were used to minimize the impact of thermal vibrations on observed atomic positions and lattice constants.

Our MD simulation of the $KNaNbOF_5$ system started as a $\sqrt{2}\times\sqrt{2}\times2$ CS phase supercell. The cell axes of the orthorhombic HT and NCS phases are oriented at an angle of 45° with respect to the two *a*-axes in the tetragonal CS phase. The $\sqrt{2}\times\sqrt{2}\times2$ transformation gives the supercell lattice an orientation that allows it to represent both CS and NCS phases, and was used for that reason. The simulation temperature was held constant at 350 °C. Pathways for reconstructive phase transitions often occur by nucleation at crystal surface structures, grain boundaries, or site defects. Consequently, MD simulations of reconstructive transitions in a bulk material often involve very high activation energies compared to experimental observations. To accelerate the CS-to-HT transition in our simulation of $KNaNbOF_5$, we found it necessary to restrict changes in two of the supercell dimensions to be unidirectional (though not driven) until the system had passed the kinetic transition barrier and would not immediately return to the CS phase configuration. After the simulation passed this threshold (∼3500 fs), the restraints were removed. To account for force contributions from the extended structure, we employed the Wolf summation method.[28] The Wolf summation method is less computationally expensive than the Ewald method for calculating the contributions from the extended structure using periodic boundary conditions, and it has been shown to give similar results when the cutoff radius is set sufficiently high.[29] We used the Wolf summation

DOI: 10.1021/jacs.6b06813
J. Am. Chem. Soc. 2016, 138, 11882−11889

method when fitting pair interaction function parameters as well as in the MD simulations.

DFT Methods. To investigate the energetics of the reaction pathway in $KNaNbOF_5$, we employ the generalized solid-state nudged elastic band (G-SSNEB).[30] The forces and stresses are evaluated with density functional theory (DFT) calculations in the general gradient approximation (GGA) of Perdew–Burke–Ernzerhof revised for solids (PBEsol),[31] as implemented in the Vienna Ab Initio Simulation Package (VASP),[32,33] with the projector augmented wave (PAW) method,[34] to treat the core and valence electrons using the following valence configurations: $3s^23p^64s^1$ for K, $2p^63s^1$ for Na, $4p^65s^14d^4$ for Nb, $2s^22p^4$ for O, and $2s^22p^5$ for F. We use a 5×5×5 Monkhorst–Pack k-point mesh,[35] with Gaussian smearing (10 meV width) for Brillouin zone (BZ) integrations and a 500 eV plane wave cutoff. Structural relaxations are performed until the Hellmann–Feynman forces are less than 10 meV $Å^{-1}$ on each atom. The free energy values were derived from the phonon vibrational frequencies using the PHONOPY package.[36]

CONCLUSION

Using a combination of empirically based MD simulations and *ab initio* DFT methods, we investigated a reconstructive phase transition in $KNaNbOF_5$, and we were able to identify the structure of the previously unsolved high-temperature phase. We found the HT phase to be structurally complex. It exhibits dynamic disorder between two phases with nearly identical cation sublattices but different orientations of the polar, heteroanionic $[NbOF_5]^{2-}$ units. We were also able to provide both a quantitative minimum energy pathway and a qualitative phenomenological model for the reconstructive process, which involves both atomic displacements and order–disorder components. Prior to the displacive component of the reconstructive transition, octahedral $[NbOF_5]^{2-}$ anionic units are observed to behave similar to rigid molecules, enabled by the covalent nature of the Nb–ligand bonds, and undergo rotation events generating an order-to-disorder transition. Disordering the O and F sites of the starting phase destabilizes the distribution of K^+ and vacant sites and provides the driving force for the displacive component of the reconstructive transition.

The reconstructive phase transition in $KNaNbOF_5$ results from the presence of a vacant site in the cation lattice. Disorder of polar heteroanionic units plays an important role, but similar behavior in related compounds with fully occupied cation lattices does lead to reconstructive transitions. The cause is therefore the combination of the vacant site in the cation lattice and the polar nature of the heteroanionic units. In a related system with half occupied and half vacant K^+ cation sites, a similar thermally induced phase transition should be observable. The compounds $KNaWO_2F_4$ and $KNaMoO_2F_4$ have been synthesized hydrothermally and are reported to fit with the space group $P4/nmm$.[15] Based on the results of our research, we conjecture that these phases should undergo thermally induced reconstructive phase transitions to HT bridging structures and cool into new and as-yet unreported polymorphs. The approach used here, combining detailed experimentation, empirically based simulations, and theoretically based analytical approaches, can provide new insights into phase transitions in other heteroanionic solid-state systems. By advancing our understanding of dynamic mechanisms that can lead systems to adopt specific structures, combined investigations like this one will lead to computational methods for suggesting the required synthetic conditions for producing targeted compounds.

ASSOCIATED CONTENT

Supporting Information

The Supporting Information is available free of charge on the ACS Publications website at DOI: 10.1021/jacs.6b06813.

Experimental crystal structure from cryogenic DAC study of ncs01q (CIF)
Experimental crystal structure from cryogenic DAC study of ncs02q (CIF)
Experimental crystal structure from cryogenic DAC study of ncs03q (CIF)
Experimental crystal structure from cryogenic DAC study of ncs04q (CIF)
Experimental crystal structure from cryogenic DAC study of ncs05q (CIF)
Theoretical crystal from MD snapshot for the *Pbcm* structure (CIF)
Theoretical crystal from MD snapshot for the *Pnma* structure (CIF)
Theoretical crystal from DFT structure optimization of the *Cmcm* structure (CIF)
Supplementary Figures 1–9, Tables S1 and S2, and equation showing the function used in the simulation to calculate the pairwise interatomic forces with the parameter values in Table S2 (PDF)

AUTHOR INFORMATION

Corresponding Author

*krp@northwestern.edu

Notes

The authors declare no competing financial interest.

ACKNOWLEDGMENTS

This work was made possible by support from the National Science Foundation (Awards DMR-1608218 and DMR-1307698). N.C. and J.M.R. acknowledge additional support from the National Science Foundation (DMR-1454688). We gratefully acknowledge Steven Jacobsen and John Lazarz for making the high-pressure experiments possible and providing the DAC. This research used resources of the Advanced Photon Source, a U.S. Department of Energy (DOE) Office of Science User Facility operated for the DOE Office of Science by Argonne National Laboratory under Contract No. DE-AC02-06CH11357. We acknowledge HPCAT, and specifically Dmitry Popov and Curtis Kenny-Benson, for assistance setting up the DAC experiments. For their help collecting the DAC data, we thank Kelvin Chang, Jacqueline Cantwell, Karl Rickert, and Robert Kennedy. For assistance and guidance during the collection of the *in situ* powder diffraction data, we thank Matthew Suchomel. DFT calculations were performed on the high-performance computing facilities available at the Center for Nanoscale Materials (CARBON Cluster) at Argonne National Laboratory, and at the Extreme Science and Engineering Discovery Environment (XSEDE), which is supported by the National Science Foundation grant no. DMR-1100085.

REFERENCES

(1) Tolédano, P.; Dmitriev, V. Reconstructive phase transitions. In *Crystals and Quasicrystals*; World Scientific: Singapore, 1996.
(2) Boulesteix, C. *Diffusionless Phase Transitions in Oxides and Some Reconstructive and Martensitic Phase Transitions*; Trans Tech Publications: New Hampshire, 1995.

DOI: 10.1021/jacs.6b06813
J. Am. Chem. Soc. 2016, 138, 11882–11889

(3) Horovitz, B.; Gooding, R.; Krumhansl, J. *Phys. Rev. Lett.* **1989**, *62*, 843.
(4) Zahn, D.; Hochrein, O.; Leoni, S. *Phys. Rev. B: Condens. Matter Mater. Phys.* **2005**, *72*, 094106.
(5) Müser, M.; Binder, K. *Phys. Chem. Miner.* **2001**, *28*, 746.
(6) Zhang, S.; Chen, N.-X. *Modell. Simul. Mater. Sci. Eng.* **2003**, *11*, 331.
(7) Pagliai, M.; Iannuzzi, M.; Cardini, G.; Parrinello, M.; Schettino, V. *ChemPhysChem* **2006**, *7*, 141.
(8) Takesada, M.; Yagi, T. *J. Phys. Soc. Jpn.* **1994**, *63*, 4282.
(9) Kusaba, K.; Yagi, T.; Kikuchi, M.; Syono, Y. *J. Phys. Chem. Solids* **1986**, *47*, 675.
(10) Xiao, P.; Cheng, J.-G.; Zhou, J.-S.; Goodenough, J. B.; Henkelman, G. *Phys. Rev. B: Condens. Matter Mater. Phys.* **2013**, *88*, 144102.
(11) Schollenbruch, K.; Woodland, A.; Frost, D.; Wang, Y.; Sanehira, T.; Langenhorst, F. *Am. Mineral.* **2011**, *96*, 820.
(12) Yang, M.; Oró-Solé, J.; Rodgers, J. A.; Jorge, A. B.; Fuertes, A.; Attfield, J. P. *Nat. Chem.* **2011**, *3*, 47.
(13) Hirose, H.; Ueda, K.; Kawazoe, H.; Hosono, H. *Chem. Mater.* **2002**, *14*, 1037.
(14) Hiraishi, M.; Iimura, S.; Kojima, K. M.; Yamaura, J.-i.; Hiraka, H.; Ikeda, K.; Miao, P.; Ishikawa, Y.; Torii, S.; Miyazaki, M.; et al. *Nat. Phys.* **2014**, *10*, 300.
(15) Pinlac, R. A. F.; Stern, C. L.; Poeppelmeier, K. R. *Crystals* **2011**, *1*, 3.
(16) Han, H.; Cheng, C.; Xiong, X.-G.; Su, J.; Dai, J.-X.; Wang, H.; Yin, G.; Huai, P. *Materials* **2015**, *8*, 8578.
(17) Chang, K. B.; Edwards, B. W.; Frazer, L.; Lenferink, E. J.; Stanev, T. K.; Stern, N. P.; Nino, J. C.; Poeppelmeier, K. R. *J. Solid State Chem.* **2016**, *236*, 78.
(18) Chang, K. B.; Vinokur, A.; Pinlac, R. A. F.; Suchomel, M. R.; Marvel, M. R.; Poeppelmeier, K. R. *Inorg. Chem.* **2014**, *53*, 6979.
(19) Stokes, H. T.; Hatch, D. M. *J. Appl. Crystallogr.* **2005**, *38*, 237.
(20) Agulyansky, A. *Chemistry of tantalum and niobium fluoride compounds*; Elsevier: Amsterdam, The Netherlands, 2004.
(21) Molokeev, M.; Misyul', S. V.; Fokina, V.; Kocharova, A.; Aleksandrov, K. *Phys. Solid State* **2011**, *53*, 834.
(22) Udovenko, A. A.; Laptash, N. M. *Acta Crystallogr., Sect. B: Struct. Sci.* **2011**, *67*, 447.
(23) Udovenko, A. A.; Laptash, N. M. *Acta Crystallogr., Sect. B: Struct. Sci.* **2008**, *64*, 527.
(24) Udovenko, A. A.; Laptash, N. M. *Acta Crystallogr., Sect. B: Struct. Sci.* **2008**, *64*, 645.
(25) Sheldrick, G. M.; Schneider, T. R. *Methods Enzymol.* **1997**, *277*, 319.
(26) Dera, P. *GSE_ADA*; GeoSoilEnviroCARS: Argonne, IL, 2007.
(27) Parrinello, M.; Rahman, A. *Phys. Rev. Lett.* **1980**, *45*, 1196.
(28) Wolf, D.; Keblinski, P.; Phillpot, S.; Eggebrecht, J. *J. Chem. Phys.* **1999**, *110*, 8254.
(29) Fennell, C. J.; Gezelter, J. D. *J. Chem. Phys.* **2006**, *124*, 234104.
(30) Sheppard, D.; Xiao, P.; Chemelewski, W.; Johnson, D. D.; Henkelman, G. *J. Chem. Phys.* **2012**, *136*, 074103.
(31) Perdew, J. P.; Ruzsinszky, A.; Csonka, G. I.; Vydrov, O. A.; Scuseria, G. E.; Constantin, L. A.; Zhou, X.; Burke, K. *Phys. Rev. Lett.* **2008**, *100*, 136406.
(32) Kresse, G.; Furthmüller, J. *Phys. Rev. B: Condens. Matter Mater. Phys.* **1996**, *54*, 11169.
(33) Kresse, G.; Joubert, D. *Phys. Rev. B: Condens. Matter Mater. Phys.* **1999**, *59*, 1758.
(34) Blöchl, P. E. *Phys. Rev. B: Condens. Matter Mater. Phys.* **1994**, *50*, 17953.
(35) Monkhorst, H. J.; Pack, J. D. *Phys. Rev. B: Condens. Matter* **1976**, *13*, 5188.
(36) Togo, A.; Oba, F.; Tanaka, I. *Phys. Rev. B: Condens. Matter Mater. Phys.* **2008**, *78*, 134106.

DOI: 10.1021/jacs.6b06813
J. Am. Chem. Soc. 2016, 138, 11882−11889